

Development and characterization of the arterial windkessel and its role during left ventricular assist device assistance

Massimo Capoccia, MD, MSc
Cardiac Surgeon
Royal Stoke University Hospital
Stoke on Trent
United Kingdom

PhD Student in Biomedical Engineering
University of Strathclyde
Glasgow
United Kingdom

Keywords: windkessel; lumped-parameter model; arterial system; LVAD

Total number of words of the manuscript: 6240

Total number of words of the abstract: 132

Number of figures: 10

Number of tables: 1

Corresponding author:

Massimo Capoccia
Email: capoccia@doctors.org.uk

This is the peer reviewed version of the following article: Capoccia, M. (2015). Development and characterization of the arterial windkessel and its role during left ventricular assist device assistance. Artificial Organs, 39(8), E138-E153. 10.1111/aor.12532, which has been published in final form at <http://dx.doi.org/10.1111/aor.12532>. This article may be used for non-commercial purposes in accordance with [Wiley Terms and Conditions for Self-Archiving](#).

Abstract

Modelling of the cardiovascular system is challenging but it has the potential to further advance our understanding of normal and pathological conditions. Morphology and function are closely related. The arterial system provides steady blood flow to each organ and damps out wave fluctuations as a consequence of intermittent ventricular ejection. These actions can be approached separately in terms of mathematical relationships between pressure and flow. Lumped parameter models are helpful for the study of the interactions between the heart and the arterial system. The arterial windkessel model still plays a significant role despite its limitations. This review aims to discuss the model and its modifications and derive the fundamental equations by applying electric circuits theory. In addition, its role during LVAD assistance is explored and discussed in relation to rotary blood pumps.

Introduction

The cardiovascular system is a dynamical closed loop driven by the heart, which is a sophisticated volume displacement pump.

Blood flow in the cardiovascular system behaves according to the laws of mass, momentum and energy conservation which are described by governing equations. Blood vessels are flexible and their constitutive equations require additional constraints that significantly influence blood flow dynamics. The ability to analyze pressure and flow wave phenomena in the arterial system as well as local blood flow characteristics is important in order to understand the development and progression of cardiovascular disorders. Modelling of the cardiovascular system is a way to obtain knowledge of pressure and flow distributions with a view to diagnosis and treatment plan [1].

The study of the cardiovascular system usually is carried out in either the time or the frequency domain. A frequency domain approach consists of linearization of the governing equations by neglecting the convective acceleration terms. Fourier or Laplace transformations are used to solve the simplified equations. Frequency domain analysis is an effective solution method but suitable for the analysis of systems where periodic motion occurs. A time domain approach is appropriate when non linear terms cannot be overlooked. Lumped- and distributed-parameter models are used for this purpose.

Lumped-parameter or zero-dimensional (0-D) models assume a uniform distribution of pressure, flow and volume within any particular compartment at any instant in time. 0-D models consist of a set of simultaneous ordinary differential equations (ODEs) representing the major components of the system such as the heart, valves and compartments of the vasculature. They are suitable for the analysis of global distributions of pressure, flow and volume over a range of physiological conditions, including the interactions between the components [2].

Distributed-parameter or higher dimensional models recognize the variation of pressure, flow and volume in space. They break up the arterial system in small segments whose geometry and mechanical properties are known. The wave-transmission properties of each arterial segment can be described using the oscillatory flow or electrical transmission line theory [3].

Distributed-parameter models consist of a set of partial differential equations: the Navier-Stokes equations. One-dimensional (1-D) models represent the effects of pulse wave transmission within the vasculature. Two-dimensional (2-D) models represent the radial variation of velocity in an axisymmetric tube. Three-dimensional (3-D) models are applicable to the study of local flow fields where fluid phenomena are complex such as near a bifurcation, within an aneurysm or in the proximity of a heart valve. 3-D models can give wall shear stress or vorticity fields but they are computationally more demanding and sensitive to boundary conditions. They involve a computational fluid dynamics (CFD) approach including fluid-structure interactions between blood and the arterial wall [4].

Combinations of models or multiscale models can be used such as 1-D models of the entire arterial system with 0-D models at the distal ends to provide realistic local boundary conditions for 3-D CFD simulations [5-7].

Model validation is critical in order to evaluate the accuracy of the assumptions by comparison with experimental and simulated data [8].

The arterial windkessel is a lumped parameter model that has been studied extensively and applied to the cardiovascular system. The aim is to discuss the model and its modifications, derive the fundamental equations by applying electric circuits theory and discuss its role in modelling the interactions between left ventricular assist devices (LVADs) and the cardiovascular system.

The Arterial Windkessel Model

The Windkessel (WK) lumped-parameter model consists of differential equations relating the dynamics of aortic pressure and blood flow to arterial compliance and resistance to blood flow.

The model assumes arteries to operate like the air-chamber in an old-fashioned hand-pumped fire engine, which smooths water pulses into continuous flow.

The WK model describes the whole arterial system in terms of pressure-flow relations at its inlet and outlet. Events that take place inside the arterial tree such as wave travel and wave reflection cannot be studied. Blood flow distribution and its changes cannot be represented. Effects of local vascular changes are not taken into account.

Despite its limitations, the WK model is easier to solve as hydraulic load on isolated hearts or assist devices in comparison with distributed models [9-13]. Also, it is an easy model to use when studying ventricular interactions and ventriculo-arterial coupling [14]. Finally, the WK model is suitable for the modelling of the systemic and pulmonary arterial systems [15].

A lumped parameter model is based on differential equations expressed in terms of hydraulic or electrical networks making it suitable to study heart failure and ventricular unloading by an assist device [16-19]. The analogy with electric circuits facilitates the formulation of the necessary equations as shown in Table 1.

Table 1

Hydraulic	Electric
Pressure (P)	Voltage (V)
Flow (Q)	Current (i)
Blood viscosity	Resistance (R)
Blood inertia	Inductance (L)
Wall compliance	Capacitance (C)

An artery can be modelled as a simple compliant tube with the assumption that its axis is rectilinear and coincident with the x axis. In the presence of laminar flow, the above parameters can be combined and approximated by linear relations as follows:

$$P = Q \cdot R \quad (\text{Ohm's Law})$$

$$Q = C \frac{dP}{dt}$$

$$P = L \frac{dQ}{dt}$$

Valves are represented as follows:

$$Q = \begin{cases} 0 & \text{if } P < P^* \\ P/R & \text{if } P \geq P^* \end{cases}$$

Where P^* is the critical pressure that needs to be overcome for the blood to flow in a preferential direction.

Kirchhoff's laws can be applied when the cardiovascular system is modelled with electrical circuits. The first law states that the sum of currents entering any junction is equal to the sum of currents leaving that junction in agreement with the conservation of blood mass. In mathematical terms, we have:

$$\sum_{n=0}^{n=\infty} I_n = 0$$

The second law states that the sum of all voltages around a loop is equal to zero in agreement with the fact that pressure is a potential difference. In mathematical terms, we have:

$$\sum_{n=0}^{n=\infty} V_n = 0$$

The 2-Element Windkessel Model

The 2-element Windkessel (2-E WK) model consists of an electrical circuit with a capacitor C as the arterial compliance and a resistor R as the peripheral resistance [20]. According to this model, the load on the heart is a combination of peripheral resistance and total arterial compliance. The 2-E WK predicts an exponential decay in diastolic pressure but the systolic relation between pressure and flow is poorly predicted [15].

If P_a is the aortic blood pressure and Q_a is the aortic blood flow, applying Kirchhoff's current law (KCL) to the circuit in Figure 1 we obtain the following differential equation:

$$Q_a = Q + \frac{P}{R} \quad (1)$$

$$\text{But: } Q = C \frac{dP}{dt} \quad (2)$$

Therefore:

$$Q_a = C \frac{dP}{dt} + \frac{P}{R} \quad (3)$$

Applying Kirchhoff's voltage law (KVL) to the left mesh of the circuit in Figure 2, we obtain:

$$P_a - P = 0 \quad (4)$$

$$\text{With } P_a = P \quad (5)$$

Figure 1

Substituting (5) in (3) and rearranging, we obtain:

$$\frac{dP_a}{dt} + \frac{P_a}{RC} = \frac{Q_a}{C} \quad (6)$$

Our integrating factor is $e^{\int dt/RC}$, then:

$$e^{\int dt/RC} \frac{dP_a}{dt} + \frac{P_a}{RC} e^{\int dt/RC} = \frac{Q_a}{C} e^{\int dt/RC}$$

$$e^{t/RC} \frac{dP_a}{dt} + \frac{P_a}{RC} e^{t/RC} = \frac{Q_a}{C} e^{t/RC}$$

$$\frac{d(P_a e^{t/RC})}{dt} = \frac{Q_a}{C} e^{t/RC} \quad (7)$$

Integrating both sides, we obtain:

$$\int d(P_a e^{t/RC}) = \frac{Q_a}{C} \int e^{t/RC} dt$$

$$P_a e^{t/RC} = \frac{Q_a}{C} RC e^{t/RC} + A$$

Finally:

$$P_a = Q_a R + A e^{-t/RC} \quad (8)$$

A is a constant of integration.

During systole, at $t = 0$, $P_a = P_0$ leading to:

$$A = P_0 - Q_a R$$

The pressure waveform for the systolic phase becomes:

$$P_a = Q_a R + (P_0 - Q_a R) e^{-t/RC}$$

Rearranging, we obtain:

$$P_a = P_0 e^{-t/RC} + Q_a R (1 - e^{-t/RC}) \quad (9)$$

During diastole, there is no inflow and $Q_a = 0$ at $t = 0$ leading to the following relationship for the diastolic phase:

$$P_a = P_0 e^{-t/RC} \quad (10)$$

The product $\tau = RC$ is the time constant, which is the time for pressure to decrease to 37% of its starting value. The larger the resistance, the slower the blood leaves the system leading to a longer time constant. In addition, the larger the compliance the more blood is stored leading again to a longer time constant. The assumption that all the compliance is located in the aorta introduces a small error because the compliance of the smaller vessels is neglected.

The term $\frac{P}{R}$ in equation (3) is a direct application of Ohm's law.

The flow out of a terminal vessel into the microcirculation is given by the following general form:

$$Q = \frac{P - P_\infty}{R}$$

Where P_∞ is the pressure related to cessation of flow through the microcirculation when arterial pressure is greater than venous pressure (waterfall effect). In other words, the vessel collapses when the upstream pressure approaches the interstitial pressure.

The inclusion of P_∞ in Equation (10) can be written in a more general form as follows:

$$P_a - P_\infty = (P_0 - P_\infty) e^{-t/RC}$$

The inclusion of P_∞ allows a better curve fitting of the arterial diastolic pressure measured in the human aorta. When $P_\infty = 0$, the failure of the model to fit the diastolic pressure waveform becomes more obvious as diastolic time increases.

The 2-E WK is a simple lumped-parameter model that gives insights into the contribution of the different arterial properties to the load on the heart but it is not suitable to reproduce systemic input impedance [21]. Computational calculations of input impedance by Fourier analysis of pressure and flow signals show the weakness of the 2-E WK model. When aortic blood flow is used as input, the model produces unrealistic aortic blood pressure wave shapes due to the poor medium- to high-frequency representation of the aortic impedance [21, 22]. At high frequencies its input impedance modulus reduces to negligible values and its phase angle reaches -90° in contrast to the aortic input impedance measured in vivo where its modulus decreases to a plateau value and the phase angle is zero degrees [15].

The 3-Element Windkessel Model

The 3-element windkessel (3-E WK) model overcomes the weakness of the 2-E WK by introducing the aortic characteristic impedance R_c , which accounts for the local inertia and local compliance of the proximal ascending aorta [23]. R_c is connected in series with the 2-E WK and can be considered as the bridging link between the lumped model and wave travel aspects of the arterial system. Although details such as the inflection point and the augmentation in aortic pressure cannot be described, the 3-E WK model produces realistic pressure and flow wave shapes with significant improvement of the medium- to high-frequency behaviour [15, 21, 23, 24].

The aortic characteristic impedance has constant modulus and phase angle of zero degrees.

At high frequencies, the input impedance equals the characteristic impedance of the proximal aorta.

The characteristic impedance is not a resistance although it is represented by a resistor. It is only present for oscillatory pressure and flow but it does not dissipate energy like a resistor. Therefore, the ratio of mean pressure over mean flow is $R + R_c$. The use of a resistor for the characteristic

impedance causes errors in the low frequency range of the input impedance [22]. However, the error is small considering that the characteristic impedance is 5-7% of the peripheral resistance in the mammalian systemic circulation [15, 25].

Applying KCL to the circuit in Figure 2, we obtain equations (1) and (3) as before.

Applying KVL to the left mesh of the circuit in Figure 2, we obtain:

$$P_a - R_c Q_a - P = 0 \quad (11)$$

Where:

$$P = P_a - R_c Q_a \quad (12)$$

Substituting (12) in (3), we obtain:

$$Q_a = C \frac{d(P_a - R_c Q_a)}{dt} + \frac{P_a - R_c Q_a}{R_p}$$

With

$$Q_a = C \frac{dP_a}{dt} - R_c C \frac{dQ_a}{dt} + \frac{P_a}{R_p} - \frac{R_c}{R_p} Q_a$$

Rearranging, we obtain:

$$C \frac{dP_a}{dt} + \frac{P_a}{R_p} = R_c C \frac{dQ_a}{dt} + \left(1 + \frac{R_c}{R_p}\right) Q_a \quad (13)$$

Figure 2

The 3-E WK model has become the most widely used and accepted lumped-parameter model of the systemic circulation. It has a limited number of physiologically meaningful parameters which offer better insight into arterial function than input impedance [15].

Although this model can produce realistic aortic pressures and flows, C tends to be overestimated and R_c underestimated. Therefore, the model works with parameter values that quantitatively differ from the vascular properties [26].

The 4-Element Windkessel Model

The 4-element windkessel (4-E WK) model overcomes the inconsistency resulting from the approximation of the characteristic impedance as a resistance by adding an inertial element L either in series or in parallel with R_c [26-29]. The inertance term equals the total inertance of the arterial system. The advantage is that the model accounts for the inertia of the whole arterial system, contributes to the low frequencies only and allows R_c intervening at medium-to-high frequencies. The 4-E WK gives a relative accurate estimation of total arterial compliance from pressure and flow.

Figure 3

When L is added in series to R_c , applying KVL to the left mesh of the circuit in Figure 3, we obtain:

$$P_a - R_c Q_a - L \frac{dQ_a}{dt} - P = 0 \quad (14)$$

Where:

$$P = P_a - R_c Q_a - L \frac{dQ_a}{dt} \quad (15)$$

Substituting (15) in (3), we obtain:

$$Q_a = C \frac{d}{dt} (P_a - R_c Q_a - L \frac{dQ_a}{dt}) + \frac{1}{R_p} (P_a - R_c Q_a - L \frac{dQ_a}{dt})$$

And

$$Q_a = C \frac{dP_a}{dt} - R_c C \frac{dQ_a}{dt} - LC \frac{d^2 Q_a}{dt^2} + \frac{P_a}{R_p} - \frac{R_c}{R_p} Q_a - \frac{L}{R_p} \frac{dQ_a}{dt}$$

Rearranging, we obtain the ODE for the circuit in Figure 3 as follows:

$$LC \frac{d^2 Q_a}{dt^2} + (R_c C + \frac{L}{R_p}) \frac{dQ_a}{dt} + (1 + \frac{R_c}{R_p}) Q_a = C \frac{dP_a}{dt} + \frac{P_a}{R_p} \quad (16)$$

When L is added in parallel to R_c , the same voltage drop (pressure drop) applies. Therefore, we obtain:

$$L \frac{dQ_L}{dt} = P_a - P \quad \text{where } P = P_a - L \frac{dQ_L}{dt} \quad (17)$$

$$Q_a - Q_L = \frac{P_a - P}{R_c} \quad \text{where } Q_L = Q_a - \frac{P_a}{R_c} + \frac{P}{R_c} \quad (18)$$

Substituting (17) in (3), we obtain:

$$Q_a = C \frac{d}{dt} (P_a - L \frac{dQ_L}{dt}) + \frac{1}{R_p} (P_a - L \frac{dQ_L}{dt})$$

Following calculations and rearranging, we have:

$$LC \frac{d^2 Q_L}{dt^2} + \frac{L}{R_p} \frac{dQ_L}{dt} + Q_a = C \frac{dP_a}{dt} + \frac{P_a}{R_p} \quad (19)$$

Substituting (18) in (19), we have:

$$LC \frac{d^2}{dt^2} (Q_a - \frac{P_a}{R_c} + \frac{P}{R_c}) + \frac{L}{R_p} \frac{d}{dt} (Q_a - \frac{P_a}{R_c} + \frac{P}{R_c}) + Q_a = C \frac{dP_a}{dt} + \frac{P_a}{R_p}$$

Following calculations and rearranging, we obtain:

$$LC \frac{d^2 Q_a}{dt^2} + \frac{L}{R_p} \frac{dQ_a}{dt} + Q_a + \frac{L}{R_c} (C \frac{d^2 P}{dt^2} + \frac{1}{R_p} \frac{dP}{dt}) = \frac{LC}{R_c} \frac{d^2 P_a}{dt^2} + (\frac{L}{R_c R_p} + C) \frac{dP_a}{dt} + \frac{P_a}{R_p} \quad (20)$$

Differentiating (3), we obtain:

$$\frac{dQ_a}{dt} = C \frac{d^2 P}{dt^2} + \frac{1}{R_p} \frac{dP}{dt} \quad (21)$$

Substituting (21) in (20), we obtain:

$$LC \frac{d^2 Q_a}{dt^2} + \frac{L}{R_p} \frac{dQ_a}{dt} + \frac{L}{R_c} \frac{dQ_a}{dt} + Q_a = \frac{LC}{R_c} \frac{d^2 P_a}{dt^2} + (\frac{L}{R_c R_p} + C) \frac{dP_a}{dt} + \frac{P_a}{R_p}$$

Multiplying both sides by $R_c R_p$ and rearranging, we obtain the ODE for the circuit in Figure 4 as follows:

$$R_c R_p C L \frac{d^2 Q_a}{dt^2} + L(R_c + R_p) \frac{dQ_a}{dt} + R_c R_p Q_a = R_p C L \frac{d^2 P_a}{dt^2} + (L + R_c R_p C) \frac{dP_a}{dt} + R_c P_a \quad (22)$$

In summary, the characteristic impedance introduces the transmission concept in the WK model improving its behaviour at high frequencies. The total arterial inertance improves the behaviour of the model at very low frequencies.

A comparison of the measured aortic input impedance with values predicted by the 2-element, 3-element and 4-element windkessel model [30] is shown in Figure 5.

Figure 4

Figure 5

The Viscoelastic Windkessel Model

Figure 6

Figure 7

The Viscoelastic Windkessel (VW) model consists of total peripheral resistance R_p in parallel with a complex and frequency dependent compliance $C_c(j\omega)$ described by a Voigt cell [31, 32]. The mechanical configuration of the Voigt cell includes a dashpot with dumping factor D in parallel with a spring with elastic constant K as shown in Figure 6. The electric analogue consists of a resistor R_d , accounting for viscous losses of wall motion, in series with a capacitor C_{VW} representing static compliance.

The VW model considers a viscoelastic rather than an elastic equivalent arterial reservoir in comparison with the 2-E WK. A comparative analysis of VW, 2-E and 3-E WK models shows that the presence of a complex and frequency dependent compliance in VW improves the interpretation of aortic input impedance and resolves conflicting compliance estimation [32].

Applying KCL to the circuit in Figure 7, we obtain:

$$Q_a = Q + \frac{P}{R_p} + \frac{P}{R_d} \quad (23)$$

$$\text{But: } Q = C \frac{dP}{dt}$$

Therefore:

$$Q_a = C \frac{dP}{dt} + \frac{P}{R_p} + \frac{P}{R_d} \quad (24)$$

Applying KVL to the left mesh of the circuit in Figure 7, we have:

$$P_a - P = 0$$

$$\text{With: } P_a = P \quad (25)$$

Substituting (25) in (24) and rearranging, we obtain:

$$C \frac{dP_a}{dt} + \left(\frac{1}{R_p} + \frac{1}{R_d} \right) P_a = Q_a \quad (26)$$

To avoid conceptual misunderstandings, the Viscoelastic Windkessel (VW) may be better defined as Viscoelastic Minimal Model (VEMM) where the hydraulic representation consists of a viscoelastic reservoir instead of an air chamber [33].

The VEMM may be considered as an alternative 3-E WK to explain the shortcomings of the 2-E WK. The static compliance of the 2-E WK explains aortic pressure decay in diastole, where the static elastic properties of the arterial wall prevail, but it falls short in systole where a faster deformation of the arterial wall occurs in response to pressure. This shortcoming is resolved by the VEMM with the introduction of the resistor R_d in series with compliance in order to develop the viscoelastic response that allows the model output to follow the rapid pressure change in systole and its slower decrease in diastole [32]. The VEMM applies aortic pressure to both the complex compliance and the total peripheral resistance during the entire cardiac cycle. In contrast with the low resistance R_c of the 3-E WK, the low resistance R_d of the VEMM does not interfere with R_p and the relation between mean

aortic pressure and cardiac output but it plays a role in modulating the arterial wall response to pulsatility [34, 35].

The overestimation of static compliance by 3-E WK may be related to elastic energy storage of the capacitor during systole in the presence of energy dissipation in the resistor R_c and discharge of the capacitor in diastole through the resistor R , which is lower than total peripheral resistance R_p .

Although 3-E WK and VEMM share the same pressure curve morphology, R_c in 3-E WK appears to behave as a viscous element necessary to reproduce the rapid pressure response in systole but its placement in series at the 2-E WK entrance causes its action to disappear in diastole, where the viscous response remains less effective.

The Inertance Viscoelastic Windkessel Model

The Inertance Viscoelastic Windkessel (IVW) model can be considered as an alternative 4-E WK consisting of an inertial element connected in series with a VW. The IVW model offers an innovative way for the interpretation of the resistive effect in terms of viscous properties of vessel wall motion [36]. According to a generalized sensitivity function analysis [37], the inductance L is suitable to represent the inertial properties of blood motion in the W4S and IVW but not in the W4P. In addition, the meaning of aortic characteristic impedance given to R_c has been put into question while R_d is likely to account for viscous losses of arterial wall motion.

Applying KCL to the circuit in Figure 8, we obtain equations (23) and (24) as before.

Applying KVL to the left mesh of the circuit in Figure 8, we have:

$$P_a - L \frac{dQ_a}{dt} - P = 0 \quad (27)$$

$$\text{With: } P = P_a - L \frac{dQ_a}{dt} \quad (28)$$

Substituting (28) in (24), we have:

$$Q_a = C \frac{d}{dt} \left(P_a - L \frac{dQ_a}{dt} \right) + \left(P_a - L \frac{dQ_a}{dt} \right) \left(\frac{1}{R_p} + \frac{1}{R_d} \right)$$

And

$$Q_a = C \frac{dP_a}{dt} - LC \frac{d^2Q_a}{dt^2} + P_a \left(\frac{1}{R_p} + \frac{1}{R_d} \right) - L \left(\frac{1}{R_p} + \frac{1}{R_d} \right) \frac{dQ_a}{dt} \quad (29)$$

Rearranging, we have:

$$LC \frac{d^2Q_a}{dt^2} + L \left(\frac{1}{R_p} + \frac{1}{R_d} \right) \frac{dQ_a}{dt} + Q_a = C \frac{dP_a}{dt} + \left(\frac{1}{R_p} + \frac{1}{R_d} \right) P_a$$

Multiplying both sides by $R_p R_d$, we obtain the ODE for the circuit in Figure 8 as follows:

$$R_p R_d LC \frac{d^2Q_a}{dt^2} + L(R_d + R_p) \frac{dQ_a}{dt} + R_p R_d Q_a = R_p R_d C \frac{dP_a}{dt} + (R_d + R_p) P_a \quad (30)$$

Again, the Inertance Viscoelastic Windkessel Model (IVW) may be better defined as Inertance Viscoelastic Minimal Model (IVEMM) to avoid misunderstandings [33]. IVEMM and W4S share the same curve morphology [36] but W4S fails to explain the significant difference observed in the development rate of R_c and R_p with a rapid reduction of R_c/R_p ratio during early vascular development [38]. This shortcoming is addressed by IVEMM where the difference observed in the development rate of R_d and R_p is similar to the findings for R_c and R_p in 4WS. Considering that R_d does not interfere with R_p and accounts for the viscous response of the arterial wall, the rapid reduction in R_d/R_p ratio during early vascular development may well be related to the continuous adaptation of viscous and elastic vessel properties to different haemodynamic conditions [36].

Figure 8

The Modified Inertance Viscoelastic Windkessel Model

The original IVW model is modified by adding a fifth element R_c , which is the characteristic impedance of the aorta in the absence of wave reflections.

Applying KVL to the left mesh of the circuit in Figure 9, we have:

$$P_a - Q_a R_c - L \frac{dQ_a}{dt} - P = 0 \quad (31)$$

$$\text{With: } P = P_a - Q_a R_c - L \frac{dQ_a}{dt} \quad (32)$$

Substituting (32) in (24), we have:

$$Q_a = C \frac{d}{dt} \left(P_a - Q_a R_c - L \frac{dQ_a}{dt} \right) + \left(\frac{1}{R_p} + \frac{1}{R_d} \right) \left(P_a - Q_a R_c - L \frac{dQ_a}{dt} \right)$$

And

$$Q_a = C \frac{dP_a}{dt} - R_c C \frac{dQ_a}{dt} - LC \frac{d^2 Q_a}{dt^2} + \left(\frac{1}{R_p} + \frac{1}{R_d} \right) P_a - R_c \left(\frac{1}{R_p} + \frac{1}{R_d} \right) Q_a - L \left(\frac{1}{R_p} + \frac{1}{R_d} \right) \frac{dQ_a}{dt} \quad (33)$$

Rearranging, we have:

$$LC \frac{d^2 Q_a}{dt^2} + \left[R_c C + L \left(\frac{1}{R_p} + \frac{1}{R_d} \right) \right] \frac{dQ_a}{dt} + \left[1 + R_c \left(\frac{1}{R_p} + \frac{1}{R_d} \right) \right] Q_a = C \frac{dP_a}{dt} + \left(\frac{1}{R_p} + \frac{1}{R_d} \right) P_a$$

Multiplying both sides by $R_p R_d$, we obtain the ODE for the circuit in Figure 9 as follows:

$$R_p R_d LC \frac{d^2 Q_a}{dt^2} + [R_p R_d R_c C + L(R_d + R_p)] \frac{dQ_a}{dt} + [R_p R_d + R_c(R_d + R_p)] Q_a = R_p R_d C \frac{dP_a}{dt} + (R_d + R_p) P_a \quad (34)$$

Figure 9

The Windkessel Model Revisited

The windkessel (reservoir) and wave theory are the two models developed in the attempt to explain the shape of arterial pressure waveform, which changes with ageing and pathological conditions. As previously discussed, the windkessel explains the pressure waveform in diastole satisfactorily but fails to model pressure changes in systole accurately. The wave theory models pressure waveform successfully but predicts the existence of "self-cancelling" forward and backward waves in diastole for which is difficult to find a biological explanation. More recently, a hybrid reservoir-wave model has been proposed as an alternative and controversial approach to arterial haemodynamics [39, 40]. The reservoir-wave theory [41-43] is based on the assumption that measured pressure and flow consist of a volume-related (reservoir/windkessel) and wave-related (excess) components. The arterial blood pressure is conveniently separated into a reservoir pressure, which accounts for the energy stored by the elastic arterial walls during systole and released in diastole, and an excess pressure, which is dependent on local conditions and is defined as the difference between the measured arterial pressure and the reservoir pressure.

In mathematical terms, we have:

$$P = P_{res} + P_{ex}$$

This approach aims to unify the analysis of systolic and diastolic haemodynamics and eliminate the apparently artefactual self-cancelling forward and backward (diastolic) waves observed with conventional wave separation [44]. Reservoir-related pressure changes should be excluded before wave motion analysis.

When the reservoir-wave theory is applied to the aorta, the pressure gradient $\frac{dP_{res}}{dt}$ must be proportional to the rate of change of volume, which is the instantaneous difference between inflow (Q_{in}) and outflow (Q_{out}) [39, 44].

As a consequence, we obtain the following equation:

$$\frac{dP_{res}}{dt} = \frac{dP}{dV} (Q_{in} - Q_{out}) \quad (35)$$

but

$$\frac{dP}{dV} = \frac{1}{C} \quad (36)$$

and

$$Q_{out} = \frac{P_{res} - P_{\infty}}{R_{res}} \quad (37)$$

where P_{∞} is the pressure at which flow through the microcirculation falls to zero (arterial asymptotic pressure).

Substituting (36) and (37) in (35), we obtain:

$$\frac{dP_{res}}{dt} = \frac{1}{C} (Q_{in} - \frac{P_{res} - P_{\infty}}{R_{res}})$$

Rearranging, we obtain the final form of the differential equation:

$$\frac{dP_{res}}{dt} = \frac{Q_{in}}{C} - \frac{P_{res} - P_{\infty}}{RC} \quad (38)$$

The analytical solution is:

$$P_{res} = P_{\infty} + (P_d - P_{\infty})e^{-t/RC} + \frac{e^{-t/RC}}{C} \int_0^t Q_{in}(t')e^{t'/RC} dt' \quad (39)$$

where Q_{in} is the flow into the aorta, P_d is the diastolic pressure at $t = 0$, P_{∞} is the arterial asymptotic pressure, C is the arterial compliance and RC is the time constant of the diastolic pressure decrease. The arterial and venous reservoir are considered hydraulic integrators of the cardiovascular system [39]. The arterial reservoir buffers the intermittent filling secondary to LV ejection by modulating arterial pressure and reservoir outflow. The venous reservoir buffers the intermittent emptying of the veins secondary to RV filling by modulating venous pressure and reservoir inflow.

The windkessel/reservoir analysis can be applied to account for the reservoir effect during LV filling [45]. The reservoir pressure is the minimum hydraulic work that the ventricle must perform in order to provide a flow waveform with the given net arterial compliance and resistance. The clinical implication of this theory relates to the integral of the excess pressure over the cardiac period as the "best" indicator of cardiac events such as myocardial infarction and stroke.

The application of reservoir-wave theory to human arterial haemodynamics has led to interesting findings [46, 47]. While forward-, backward- and reservoir pressure increase with age, the increase in backward pressure is very small and its contribution to the overall pressure is unlikely to account for the large changes in pressure augmentation observed with aging and in pathological conditions. This interpretation challenges the widely accepted wave-reflection mechanism of pressure augmentation, which does not take into account the "cushioning" effect of the aortic reservoir but only the reflected waves returning from the distal aorta [39, 40].

The new approach may well contribute to further develop our understanding of the cardiovascular system but is certainly generating quite a debate [40, 48]. Criticism has been raised about inconsistency in the formulation of P_{res} and the validity of modified wave analysis using P_{ex} [48-52].

LVADs Modelling

Ventricular assist devices (VADs) are designed to support a failing heart with a view to recovery, bridge to transplant or long-term treatment. Broadly speaking, there are two main categories of mechanical blood pumps: volume-displacement and rotary pumps.

Volume-displacement pumps consist of a chamber or a sac that fills passively or by suction and is compressed by an external pusher plate. Energy is transferred to the blood by periodic changes in a working space generating pulsatile flow. Inflow and outflow prosthetic valves are required. Devices such as HeartMate I XVE and Novacor are based on this principle.

Rotary blood pumps can be axial, radial (centrifugal) and diagonal (mixed flow) according to the geometry of the impeller. Energy is transferred to the blood by velocity changes within the impeller vanes generating non-pulsatile flow. Axial flow pumps (HeartMate II and Jarvik 2000) are driven by a spinning rotor around a central shaft. Centrifugal flow pumps (HeartWare and DuraHeart) are driven by a hydrodynamic or electromagnetic suspended spinning rotor. Rotary blood pumps are suitable for high flows up to 20 l/min at differential pressures lower than 500 mmHg. The radial design is capable of producing high pressures and low flows. An axial flow pump generates high flows at low pressure differences. A diagonal pump is a mixed flow system capable of generating high pressures and high flows. Pump design is normalized to pump size taking into account that a 60-mm-diameter centrifugal pump can eject more fluid at significantly higher pressures than a 6-mm-diameter axial pump.

Volume-displacement pumps are known as *first generation devices*. Their performance is excellent at unloading the left ventricle and sustaining the circulation with a capacity to pump up to 10 L/min of pulsatile flow. However, there are clear disadvantages such as large size, complexity, noisy operating mode and limited durability because of many moving parts [53, 54]

Rotary pumps with continuous axial flow requiring mechanical bearings and seals in contact with blood are known as *second generation devices*. They are smaller and safer to insert with more favourable durability because of only one moving part. Thrombus formation remains a feared complication and varies between pumps. Experience with this type of devices is well established [55-58]. Rotary pumps with continuous flow based on magnetic levitation or non-contacting hydrodynamic bearings allowing the impeller to be suspended are known as *third generation devices*. These pumps are based on the concept of centrifugal flow and are even smaller than axial flow pumps. The use of magnetically levitated rotor systems is likely to improve durability. HeartWare and DuraHeart are two emerging devices based on this principle. Although clinical experience with these pumps is just getting under way, early results are promising [59-62].

A ventricular assist device consists of a pump with an inflow and an outflow cannulae.

Energy loss secondary to pressure drop in both cannulae as a result of viscous loss is simulated by adding a resistive component to the model. An inductance component is added to account for the additional pressure drop observed in a pulsatile flow device because of the acceleration and deceleration of blood flow. This is also applicable to continuous flow devices where the interaction between the heart and the varying pressure head may generate pulsatile pump flow.

A rotary blood pump can be modelled either considering the hydraulic component only or including the motor component too. Modelling hydraulic and motor component together may be a more useful approach because of the relation between the pump model and measurable parameters following device implantation such as power consumption and rotational speed.

The flow generated by rotary blood pumps depends on the pressure head in contrast to displacement pumps where preload and afterload are independent factors.

The traditional approach is to model rotary blood pumps using static performance curves, which relate flow rate and pressure head at different constant speed under steady conditions. According to Euler's equation, the pump pressure head can be estimated by a linear relationship with the flow rate and a quadratic relationship with the rotational speed as follows:

$$H = a_1 Q + c_1 \omega^2 \quad (40)$$

In order to improve the accuracy of pressure head estimation, additional parameters have been added such as a quadratic function of the flow rate to account for viscous loss across the pump, the time derivative of flow rate for energy loss secondary to fluid inertia and time derivative of rotational speed for pulsating operation mode [63-67]. The outcome is consistent with improved accuracy as shown by curve fitting and statistical analysis [68] although complexity is increased.

The above parameters can be combined as follows [68]:

$$H = a_2 Q + b_2 Q^2 + c_2 \omega^2 \quad (41)$$

$$H = a_3Q + b_3Q^2 + c_3\omega^2 + e_3 \frac{d\omega}{dt} \quad (42)$$

$$H = a_4Q + b_4Q^2 + c_4\omega^2 + d_4 \frac{dQ}{dt} \quad (43)$$

$$H = a_5Q + b_5Q^2 + c_5\omega^2 + d_5 \frac{dQ}{dt} + e_5 \frac{d\omega}{dt} \quad (44)$$

where H, Q and ω are functions of time.

The above equations can be applied in order to model some of the pumps currently used in clinical practice.

An axial flow pump can be characterized by the relation between pressure difference, flow and speed [69, 70]. Under steady state conditions, a linear relationship with the flow and a quadratic relationship with the pump speed are observed. In mathematical terms, we have:

$$H = P_o - P_i = b_0Q + b_1 \frac{dQ}{dt} + b_2\omega^2 \quad (45)$$

Where P_o and P_i are pressures at the outlet and the inlet of the pump; $\frac{dQ}{dt}$ is the time derivative of flow; b_0, b_1 and b_2 are pump-dependent constant coefficients. The pressure difference is linearly dependent on flow derivative. The model identifies the characteristics of the pump and the state variables related to its operation and provide estimates of flow and pressure difference of the axial pump.

An alternative approach is to model pump and cannulae separately [63, 64, 71, 72]. Only the hydraulic component of the pump is modelled and the rotational speed of the impeller is the only pump parameter that can be set by the user. The pump is in parallel with the left ventricle and a 4-element windkessel is used for the coupling with the circulation. The model is based on the more frequently used surgical approach: inflow cannula through the apex of the left ventricle and outflow cannula to the ascending aorta as an end-to-side anastomosis. The cannulae have a cylindrical shape. A rotary blood pump can be considered as a series combination of an ideal pressure source and a resistive component that models energy loss. Therefore, the pump is modelled as the sum of two terms: one as a function of the rotational speed (generated energy) and the other as a function of the flow (energy loss). The HeartMate II and the HeartWare HVAD are rotary blood pumps that fulfil the above features.

The equations describing the two pumps and their cannulae are as follows:

$$H_p = R_pQ + L_p \frac{dQ}{dt} + \beta\omega^2 \quad (46)$$

$$H_i = R_iQ + L_i \frac{dQ}{dt} \quad (47)$$

$$H_o = R_oQ + L_o \frac{dQ}{dt} \quad (48)$$

where H_p is the pressure difference (pressure head) ($mmHg$) across the pump; H_i and H_o are the pressure difference across the inlet and outlet cannulae; Q is the blood flow (l/min) through the pump and the cannulae; R_p and L_p are the pump resistance ($mmHg \cdot min^2/l^2$) and inertance ($mmHg \cdot min^2/l$); R_i and L_i are the resistance and the inertance of the inflow cannula; R_o and L_o are the resistance and the inertance of the outflow cannula; ω is the pump rotational speed (rpm) and β is a pump-dependent constant coefficient ($mmHg/rpm^2$).

The governing equation of the LVAD is the sum of the pressure difference across the inflow cannula, the pump and the outflow cannula (Figure 10) according to the following equation:

$$\Delta P = H = H_i + H_p + H_o = (R_i + R_p + R_o)Q + (L_i + L_p + L_o) \frac{dQ}{dt} + \beta\omega^2 \quad (49)$$

Considering that $\Delta P = P_{Ao} - P_{LV}$; $R = R_i + R_p + R_o$ and $L = L_i + L_p + L_o$, the final equation becomes:

$$P_{Ao} - P_{LV} = R \cdot Q + L \frac{dQ}{dt} + \beta\omega^2 \quad (50)$$

where P_{Ao} is the aortic pressure ($mmHg$), P_{LV} is the left ventricular pressure ($mmHg$), R is the total flow-dependent resistance ($mmHg \cdot min^2/l^2$) and L is the total inertance ($mmHg \cdot min^2/l$).

VADs operate in the transitional region at the boundary of laminar and turbulent flow (low Reynolds number). If the pump flow pattern is expected to be turbulent, then the pump pressure loss is related to the square of the flow. The LVAD governing equation becomes:

$$P_{Ao} - P_{LV} = R \cdot Q^2 + L \frac{dQ}{dt} + \beta \omega^2 \quad (51)$$

Continuous flow blood pumps operate at constant speed with a flow waveform related to the waveform of the pressure difference between the pump inlet (left ventricular pressure) and outlet (aortic pressure) [66, 73]. Therefore, the pump flow is affected by the pulsatility of the left ventricular pressure and the features of the pump itself.

Figure 10

A basic model assumes the right ventricle and the pulmonary circulation to be normal; therefore, their effect on the LVAD is negligible. The left ventricle is modelled with a time varying compliance $C(t)$, which is the reciprocal of the ventricular elastance function $E(t)$. In mathematical terms, we obtain:

$$E(t) = \frac{P_{LV}(t)}{V_{LV}(t) - V_0} \quad (52)$$

Where $P_{LV}(t)$ is the left ventricular pressure, $V_{LV}(t)$ is the left ventricular volume and V_0 is the theoretical ventricular volume at zero pressure.

A Lagrange multiplier coupling approach [74] can be applied to LVAD modelling [75] using fictitious domain methods [76, 77] to address the interactions between the LVAD cannula and the ventricle at the expense of significant increase in computational time. These challenging aspects may be overcome with a 0D windkessel [78-81]. A windkessel model and a time-varying resistance have been used more recently for dynamic modelling of pulsatile pumps [82].

Discussion

The contentious issue is whether forward and backward pressure waves in the arterial system represent reality. The current view [83] is that wave reflection exists and is caused mainly by the termination of low resistance arteries into high resistance arterioles resulting in the two major components of the arterial pressure wave [84-87]. This is the view shared by clinicians and physiologists [88] where wave reflection is considered as optimally timed in young humans but progressively mistimed in advanced age as the aorta stiffens [83].

Windkessel models do not take pressure wave reflection into account but a practical application of the 3-element windkessel gives accurate computed aortic flow pulsations from arterial pressure during cardiopulmonary bypass [89] and in patients with septic shock [90].

The reservoir-wave approach proposes a different formulation of the 2-element windkessel model [91]. The theoretical background of the reservoir-wave approach is based on a reduced form of the wave equations (one-dimensional Navier-Stokes). It is argued [49] that dividing pressure into "reservoir" and wave components is theoretically problematic because reservoir and wave effects are not mutually exclusive: any phenomena viewed as a reservoir effect must also be explicable in terms of waves [50-52]. A recent comparison between reservoir-wave approach and traditional wave analyses in physiological numerical models containing well-defined impedance mismatches seems to favour the traditional approach [50, 51]. In contrast, impedance analysis assumes a steady-state system oscillating around mean pressure and cannot address to what extent waves from previous systole contribute to mean arterial pressure [92].

Arterial wave phenomena are spread across the entire wavelength range making quantitative interpretation of pressure and flow waveforms prone to error by using simple wave guide or windkessel models. Arterial blood pressure waveforms are the result of the interaction between ventricle and arterial system which show non-linear and time-dependent behaviour. Integration of ventricular and vascular concepts may lead to a more system-oriented interpretation of clinical measurements.

The reservoir-wave approach may be considered as a time-domain representation of the 3-element windkessel model [93]. The 3-element windkessel describes input impedance and system behaviour

as a whole [23] while the reservoir-wave approach separates wave from reservoir component [94]. Given the successful application of a 0D windkessel in LVAD modelling [78-81], the reservoir-wave approach may have a role to play.

From a clinical point of view, it is difficult to answer whether forward and backward wave reflection represent reality because most interventional procedures affect both cardiac output and peripheral resistance with concomitant changes in forward and backward pressure waves. Forward pressure waves seem to play a major role in normal physiology compared to backward waves [95, 96]. A relative shift from forward to backward waves occurs in heart failure [97], which may be an attractive setting to study the reality of backward pressure waves. In fact, reflection magnitude, calculated as the ratio of backward to forward wave, has been identified as an important predictor of cardiovascular events in heart failure patients [98].

At present, there is no simple model that captures all the required elements in order to provide a full view of arterial wave travel and reflection [52]. The duality wave-particle of light is a very well established concept in physics. The same may be considered in haemodynamics where the two approaches would apply accordingly.

Concluding Remarks

The windkessel model is a simple and useful concept although in contrast with the modern approaches that interpret arterial pressure and flow waveforms in terms of wave propagation and reflection. Despite its limitations, the windkessel remains a widely used lumped parameter model for the cardiovascular system, particularly successful for the study of the interactions following the insertion of a left ventricular assist device. The reservoir-wave theory is a controversial alternative with potential for clinical application. This is a stimulating and exciting development that is certainly generating a debate but it may well contribute to further develop a different approach to LVAD modelling.

Disclosures: none

Acknowledgements

I am very grateful to Prof. KH Parker for his precious suggestions. I am also grateful to Katharine H Fraser from Imperial College in London who allowed me to use and modify her electrical circuit model.

References

- 1 van de Vosse FN, Stergiopoulos N. Pulse Wave Propagation in the Arterial Tree. *Annu Rev Fluid Mech* 2011; 43: 467-499.
- 2 Shi Y, Lawford P, Hose R. Review of Zero-D and 1-D Models of Blood Flow in the Cardiovascular System. *Biomedical Engineering OnLine* 2011; 10: 33-70.
- 3 Womersley JR. Method for the calculation of velocity, rate of flow and viscous drag in arteries when the pressure gradient is known. *J Physiol* 1955; 127: 553-563.
- 4 Heil M, Hazel AL. Fluid-Structure Interaction in Internal Physiological Flows. *Annu Rev Fluid Mech* 2011; 43: 141-162.
- 5 Beulen BWAMM, Rutten MCM, van de Vosse FN. A time-periodic approach for fluid-structure interaction in distensible vessels. *J Fluids Struct* 2009; 25(5): 954-966.
- 6 Quarteroni A, Veneziani A. Analysis of a Geometrical Multiscale Model Based on the Coupling of ODEs and PDEs for Blood Flow Simulations. *Multiscale Model Simul* 2003; 1(2): 173-195.
- 7 Taylor CA, Figueroa CA. Patient-Specific Modelling of Cardiovascular Mechanics. *Annu Rev Biomed Eng* 2009; 11: 109-134.
- 8 Kokalari I, Karaja T, Guerrisi M. Review on lumped parameter method for modelling the blood flow in systemic arteries. *J Biomedical Science and Engineering* 2013; 6: 92-99.
- 9 Westerhof N, Bosman F, De Vries CJ, Noordergraaf A. Analog studies of the human systemic arterial tree. *J Biomechanics* 1969; 2: 121-143.
- 10 O'Rourke MF, Avolio AP. Pulsatile flow and pressure in human systemic arteries. Studies in man and in a multibranch model of the human systemic arterial tree. *Circ Res* 1980; 46: 363-372.
- 11 Stergiopoulos N, Young DF, Rodge TR. Computer simulation of arterial flow with applications to arterial and aortic stenoses. *J Biomechanics* 1992; 25(12): 1477-1488.
- 12 Ferrari G, Kozarski M, De Lazzari C, Gorczyńska K, Darowski M, Tosti G. Development of Hybrid (Numerical-Physical) Models of the Cardiovascular System: Numerical-Electrical and Numerical Hydraulic Applications. *Biocybernetics and Biomedical Engineering* 2005; 25(4): 3-15.
- 13 Ferrari G, Kozarski M, De Lazzari C, Gorczyńska K, Palko KJ, Zielinski K, Di Molfetta A, Darowski M. Role and Applications of Circulatory Models in Cardiovascular Pathophysiology. *Biocybernetic and Biomedical Engineering* 2009; 29(4): 3-24.
- 14 Luo C, Ware DL, Zwischenberger JB, Clark JW Jr. Using a Human Cardiopulmonary Model to Study and Predict Normal and Diseased Ventricular Mechanics, Septal Interaction, and Atrio-Ventricular Blood Flow Patterns. *Cardiovasc Eng* 2007; 7: 17-31.
- 15 Westerhof N, Lankhaar J-W, Westerhof BE. The arterial Windkessel. *Med Biol Eng Comput* 2009; 47: 131-141.
- 16 Wang Y, Loghmanpour N, Vandenberghe S, Ferreira A, Keller B, Gorcsan J, Antaki J. Simulation of Dilated Heart Failure with Continuous Flow Circulatory Support. *PLoS ONE* 2014; 9(1): e85234.
- 17 Gohean JR, George MJ, Pate TD, Korusz M, Longoria RG, Smalling RW. Verification of a Computational Cardiovascular System Model Comparing the Hemodynamics of a Continuous Flow to a Synchronous Valveless Pulsatile Flow Left Ventricular Assist Device. *ASAIO Journal* 2013; 59: 107-116.

- 18 McCormick M, Nordsletten DA, Kay D, Smith NP. Simulating left ventricular fluid-solid mechanics through the cardiac cycle under LVAD support. *Journal of Computational Physics* 2013; 244: 80-96.
- 19 Lim E, Dokos S, Salamonsen RF, Rosenfeldt FL, Ayre PJ, Lovell NH. Numerical Optimization Studies of Cardiovascular-Rotary Blood Pump Interaction. *Artificial Organs* 2012; 36(5): E110-E124.
- 20 Frank O. Die Grundform des arteriellen Pulses, Erste Abhandlung: Mathematische Analyse. *Zeitschrift für Biologie* 1899; 37: 483-526.
- 21 Stergiopoulos N, Meister JJ, Westerhof N. Evaluation of methods for the estimation of total arterial compliance. *Am J Physiol Heart Circ Physiol* 1995; 268: H1540-1548.
- 22 Stergiopoulos N, Meister JJ, Westerhof N. Simple and accurate way for estimating total and segmental arterial compliance: the pulse pressure method. *Ann Biomed Eng* 1994; 22: 392-397.
- 23 Westerhof N, Elzinga G, Sipkema P. An artificial arterial system for pumping hearts. *J Appl Physiol* 1971; 31: 776-781.
- 24 Toorop GP, Westerhof N, Elzinga G. Beat-to-beat estimation of peripheral resistance and arterial compliance during pressure transients. *Am J Physiol Heart Circ Physiol* 1987; 252: H1275-H1283.
- 25 Westerhof N, Elzinga G. Normalized input impedance and arterial decay time over heart period are independent of animal size. *Am J Physiol Regul Integr Comp Physiol* 1991; 261(1): R126-R133.
- 26 Stergiopoulos N, Westerhof BE, Westerhof N. Total arterial inertance as the fourth element of the windkessel model. *Am J Physiol Heart Circ Physiol* 1999; 276: H81-H88.
- 27 Burattini R, Gnudi G. Computer identification of models for the arterial tree input impedance: Comparison between two new simple models and first experimental results. *Med Biol Eng Comput* 1982; 20: 134-144.
- 28 Campbell KB, Ringo JA, Neti C, Alexander JE. Informational analysis of left ventricle-systemic arterial interaction. *Ann Biomed Eng* 1984; 12: 209-231.
- 29 Cole RT, Lucas CL, Cascio WE, Johnson TA. A LabVIEW™ Model Incorporating an Open-Loop Arterial Impedance and a Closed-Loop Circulatory System. *Ann Biomed Eng* 2005; 33(11): 1555-1573.
- 30 Segers P, Rietzschel ER, De Buyzere ML, Stergiopoulos N, Westerhof N, Van Bortel LM, Gillebert T, Verdonck PR. Three- and four-element Windkessel models: assessment of their fitting performance in a large cohort of healthy middle-aged individuals. *Proceedings of the Institution of Mechanical Engineers, Part H: Journal of Engineering in Medicine* 2008; 222: 417-428.
- 31 Burattini R, Campbell KB. Effective distributed compliance of the canine descending aorta estimated by modified T-tube model. *Am J Physiol Heart Circ Physiol* 1993; 264: H1977-H1987.
- 32 Burattini R, Natalucci S. Complex and frequency-dependent compliance of viscoelastic windkessel resolves contradictions in elastic windkessels. *Medical Engineering & Physics* 1998; 20: 502-514.
- 33 Burattini R. Downstream from the Heart Left Ventricle: Aortic Impedance Interpretation by Lumped and Tube-Load Models. In: Carson E, Cobelli C (eds) *Modelling Methodology for Physiology and Medicine*, pp 503-525. Elsevier Inc., 2014.
- 34 Burattini R, Montanari L, Mulligan LJ, Cannon MS, Gross DR. Evaluation of hypercholesterol diet-induced changes in visco-elastic properties of carotid circulation in pigs. *Am J Physiol Heart Circ Physiol* 1992; 263: H1919-H1926.

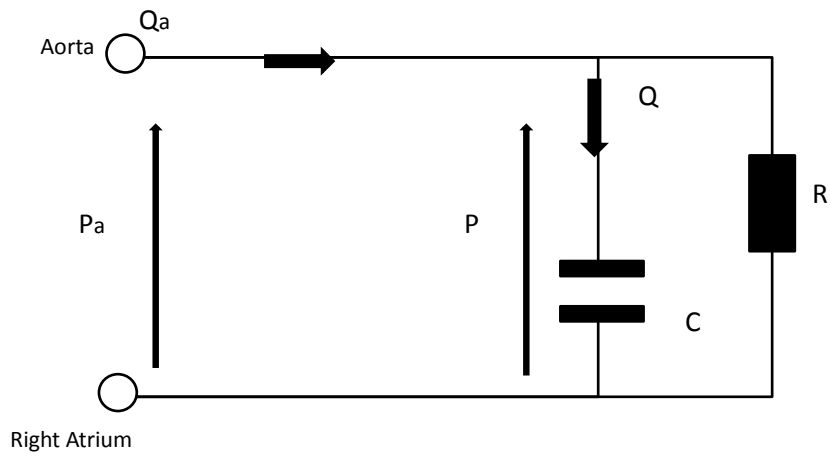
- 35 Burattini R, Natalucci S, Campbell KB. Visco-elasticity modulates resonance in the terminal aortic circulation. *Med Eng Phys* 1999; 21: 175-185.
- 36 Burattini R, Di Salvia PO. Development of systemic arterial mechanical properties from infancy to adulthood interpreted by four-element windkessel models. *J Appl Physiol* 2007; 103: 66-79.
- 37 Burattini R, Bini S. Physiological interpretation of inductance and low-resistance terms in four-element windkessel models: Assessment by generalized sensitivity function analysis. *Medical Engineering & Physics* 2011; 33: 739-754.
- 38 Sharp MK, Pantalos GM, Minich L, Tani LY, McGough EC, Hawkins JA. Aortic input impedance in infants and children. *J Appl Physiol* 2000; 88: 2227-2239.
- 39 Tyberg JV, Davies JE, Wang Z, Whitelaw WA, Flewitt JA, Shrive NG, Francis DP, Hughes AD, Parker KH, Wang J-Jr. Wave intensity analysis and the development of the reservoir-wave approach. *Med Biol Eng Comput* 2009; 47(2): 221-32.
- 40 Tyberg JV, Bouwmeester JC, Parker KH, Shrive NG, Wang J-Jr. The case for the reservoir-wave approach. *International Journal of Cardiology* 2014; 172: 299-306.
- 41 Wang JJ, O'Brien AB, Shrive NG, Parker KH, Tyberg JV. Time-domain representation of ventricular-arterial coupling as a windkessel and wave system. *Am J Physiol Heart Circ Physiol* 2003; 284: H1358-H1368.
- 42 Wang JJ, Flewitt JA, Shrive NG, Parker KH, Tyberg JV. Systemic venous circulation. Waves propagating on a windkessel: relation of arterial and venous windkessels to systemic vascular resistance. *Am J Physiol Heart Circ Physiol* 2006; 290: H154-H162.
- 43 Wang JJ, Shrive NG, Parker KH, Hughes AD, Tyberg JV. Wave Propagation and Reflection in the Canine Aorta: Analysis Using a Reservoir-Wave Approach. *Can J Cardiol* 2011; 27(3): 389.e1 – 389.e10.
- 44 Davies JE, Hadjiloizou N, Leibovich D, Malaweera A, Alastruey-Armon J, Whinnett ZI, Manisty CH, Francis DP, Aguado-Sierra J, Foale RA, Malik IS, Parker KH, Mayet J, Hughes AD. Importance of the aortic reservoir in determining the shape of the arterial pressure waveform - the forgotten lessons of Frank. *Artery Res* 2007; 1: 40-45.
- 45 Flewitt JA, Hobson TN, Wang JJ, Johnston CF, Shrive NG, Belenkie I, Parker KH, Tyberg JV. Wave intensity analysis of left ventricular filling: application of windkessel theory. *Am J Physiol Heart Circ Physiol* 2007; 292: H2817-H2823.
- 46 Davies JE, Whinnett ZI, Francis DP, Manisty CH, Aguado-Sierra J, Willson K, Foale RA, Malik IS, Hughes AD, Parker KH, Mayet J. Evidence of a dominant backward-propagating "suction" wave responsible for diastolic coronary filling in humans, attenuated in left ventricular hypertrophy. *Circulation* 2006; 113: 1768-1778.
- 47 Davies JE, Francis DP, Manisty CH, Hadjiloizou N, Aguado-Sierra J, Malik IS, Foale RA, Hughes AD, Parker KH, Mayet J. A unifying explanation of the aortic pulse waveform in humans. *J Am Coll Cardiol* 2007; 49(9) Suppl 1: 397A-398A.
- 48 Mynard JP, Smolich JJ. The case against the reservoir-wave approach. *International Journal of Cardiology* 2014; 176(3): 1009-1012.
- 49 Mynard JP, Smolich JJ. The reservoir-wave paradigm may be plausible, but is it valid? *Published on line March 20, 2013* Comments on the CrossTalk proposal and opposing view: Forward and backward pressure waves in the arterial system do/do not represent reality. *J Physiol* 2013; 591(5): 1167-1177.
- 50 Mynard JP, Penny DJ, Davidson MR, Smolich JJ. The reservoir-wave paradigm introduces error into arterial wave analysis: a computer modelling and in-vivo study. *J Hypert* 2012; 30: 734-743.

- 51 Mynard JP, Penny DJ, Davidson MR, Smolich JJ. The reservoir-wave paradigm. *J Hypert* 2012; 30: 1881-1883.
- 52 Segers P, Mynard J, Taelman L, Vermeersch S, Swillens A. Wave reflection: myth or reality? *Artery Res* 2012; 6: 7-11.
- 53 Birks EJ, Tansley PD, Yacoub MH, Bowles CT, Hipkin M, Hardy J, Banner NR, Khaghani A. Incidence and Clinical Management of Life-Threatening Left Ventricular Assist Device Failure. *J Heart Lung Transplant* 2004; 23: 964-969.
- 54 Pagani FD, Long JW, Dembitsky WP, Joyce LD, Miller LW. Improved Mechanical Reliability of the HeartMate XVE Left Ventricular Assist System. *Ann Thorac Surg* 2006; 82: 1413-1418.
- 55 Miller LW, Pagani FD, Russell SD, John R, Boyle AJ, Aaronson KD, Conte JV, Naka Y, Mancini D, Delgado RM, MacGillivray TE, Farrar DJ, Frazier OH for the HeartMate II Clinical Investigators. Use of a Continuous-Flow Device in Patients Awaiting Heart Transplantation. *N Engl J Med* 2007; 357: 885-896.
- 56 Pagani FD, Miller LW, Russell SD, Aaronson KD, John R, Boyle AJ, Conte JV, Bogaev RC, MacGillivray TE, Naka Y, Mancini D, Massey HT, Chen L, Klodell CT, Aranda JM, Moazami N, Ewald GA, Farrar DJ, Frazier OH, HeartMate II Investigators. Extended Mechanical Circulatory Support With a Continuous-Flow Rotary Left Ventricular Assist Device. *J Am Coll Cardiol* 2009; 54: 312-321
- 57 Slaughter MS, Rogers JG, Milano CA, Russell SD, Conte JV, Feldman D, Sun B, Tatrooles AJ, Delgado RM III, Long JW, Wozniak TC, Ghumman W, Farrar DJ, Frazier OH for the HeartMate II Investigators. Advanced Heart Failure Treated with Continuous-Flow Left Ventricular Assist Device. *N Engl J Med* 2009; 361: 2241-2251.
- 58 Sheikh FH, Russell SD. HeartMate® II continuous-flow left ventricular assist system. *Expert Rev Med Devices* 2011; 8: 11-21.
- 59 Tuzun E, Roberts K, Cohn WE, Sargin M, Gemmato CJ, Radovancevic B, Frazier OH. In Vivo Evaluation of the HeartWare Centrifugal Ventricular Assist Device. *Tex Heart Inst J* 2007; 34: 406-411.
- 60 Morshuis M, El-Banayosy A, Arusoglu L, Koerfer R, Hetzer R, Wieselthaler G, Pavie A, Nojiri C. European experience of Duraheart™ magnetically levitated centrifugal left ventricular assist system. *Eur J Cardiothorac Surg* 2009; 35: 1020-1028.
- 61 Wieselthaler GM, O'Driscoll G, Jansz P, Khaghani A, Strueber M for the HVAD Clinical Investigators. Initial clinical experience with a novel left ventricular assist device with a magnetically levitated rotor in a multi-institutional trial. *J Heart Lung Transplant* 2010; 29: 1218-1225.
- 62 Strueber M, O'Driscoll G, Jansz P, Khaghani A, Levy WC, Wieselthaler GM for the HeartWare Investigators. Multicenter Evaluation of an Intrapericardial Left Ventricular Assist System. *J Am Coll Cardiol* 2011; 57: 1375-1382.
- 63 Vandenberghe S, Segers P, Meyns B, Verdonck PR. Effect of Rotary Blood Pump Failure on Left Ventricular Energetics Assessed by Mathematical Modelling. *Artificial Organs* 2002; 26(12): 1032-1039.
- 64 Vandenberghe S, Segers P, Meyns B, Verdonck PR. Unloading Effect of a Rotary Blood Pump Assessed by Mathematical Modelling. *Artificial Organs* 2003; 27(12): 1094-1101.
- 65 Gwak K-W, Ricci M, Snyder S, Paden BE, Boston JR, Simaan MA, Antaki JF. In Vitro Evaluation of Multiobjective Hemodynamic Control of a Heart-Assist Pump. *ASAIO Journal* 2005; 51: 329-335.
- 66 Moscato F, Danieli GA, Schima H. Dynamic modelling and identification of an axial flow ventricular assist device. *International Journal of Artificial Organs* 2009; 32: 336-343.

- 67 Shu F, Vandenberghe S, Antaki JF. The Importance of dQ/dt on the Flow Field in a Turbodynamic Pump With Pulsatile Flow. *Artificial Organs* 2009; 33: 757-762.
- 68 Pirbodaghi T, Weber A, Carrel T, Vandenberghe S. Effect of Pulsatility on the Mathematical Modelling of Rotary Blood Pumps. *Artificial Organs* 2011; 35(8): 825-832.
- 69 Choi S, Boston JR, Thomas D, Antaki JF. Modelling and Identification of an Axial Flow Pump. *Proceedings of the American Control Conference, Albuquerque, New Mexico, 1997, 3714-3715.*
- 70 Giridharan GA, Skliar M, Olsen DB, Pantalos GM. Modelling and Control of a Brushless DC Axial Flow Ventricular Assist Device. *ASAIO Journal* 2002; 48: 272-289.
- 71 Simaan MA. Rotary Heart Assist Devices. In: *Handbook of Automation (Nof SY, ed.) pp. 1409-1422. Springer, 2009.*
- 72 Simaan MA, Faragallah G, Wang Y, Divo E. Left Ventricular Assist Devices: Engineering Design Considerations. In: *New Aspects of Ventricular Assist Devices (Reyes G, ed) pp. 21-42. InTech, 2011.*
- 73 Granegger M, Moscato F, Casas F, Wieselthaler G, Schima H. Development of a Pump Flow Estimator for Rotary Blood Pumps to Enhance Monitoring of Ventricular Function. *Artificial Organs* 2012; 36: 691-699.
- 74 Nordsletten D, Kay D, Smith N. A non-conforming monolithic finite element method for problems of coupled mechanics. *Journal of Computational Physics* 2010; 229: 7571-7593.
- 75 McCormick M, Nordsletten D, Kay D, Smith N. Modelling left ventricular function under assist device support. *International Journal for Numerical Methods in Biomedical Engineering* 2011; 27: 1073-1095.
- 76 Baaijens FP. A fictitious domain/mortar element method for fluid-structure interaction. *International Journal for Numerical Methods in Fluids* 2001; 35: 743-761.
- 77 van Loon R, Anderson PD, van de Vosse FN. A fluid-structure interaction method with solid-rigid contact for heart valve dynamics. *Journal of Computational Physics* 2006; 217: 806-823.
- 78 Shi Y, Korakianitis T. Numerical Simulation of Cardiovascular Dynamics With Left Heart Failure and In-series Pulsatile Ventricular Assist Device. *Artificial Organs* 2006; 30(12): 929-948.
- 79 Shi Y, Korakianitis T, Bowles C. Numerical simulation of cardiovascular dynamics with different types of VAD assistance. *Journal of Biomechanics* 2007; 40: 2919-2933.
- 80 McCormick M, Nordsletten DA, Kay D, Smith NP. Simulating left ventricular fluid-solid mechanics through the cardiac cycle under LVAD support. *Journal of Computational Physics* 2013; 244: 80-96.
- 81 De Lazzari C, Ferrari G. Right Ventricular Assistance by Continuous Flow Device. A Numerical Simulation. *Methods Inf Med* 2007; 46: 530-537.
- 82 Huang H, Yang M, Wu S, Liao H. Dynamic modelling of the outlet of a pulsatile pump incorporating a flow-dependent resistance. *Medical Engineering & Physics* 2013; 35: 1097-1104.
- 83 O'Rourke MF, Nichols WW, Vlachopoulos C. CrossTalk: Wave reflection and The Physiological Society. *Published on line April 8, 2013* Comments on the CrossTalk proposal and opposing view: Forward and backward pressure waves in the arterial system do/do not represent reality. *J Physiol* 2013; 591(5): 1167-1177.
- 84 McDonald DA, Taylor MG. The hydrodynamics of the arterial circulation. *Progr Biophys Chem* 1959; 9: 107-173.

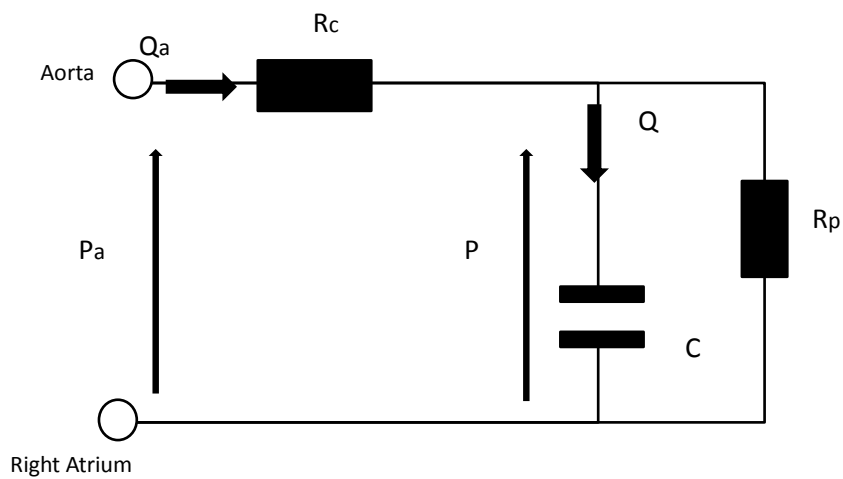
- 85 McDonald DA. *Blood Flow in Arteries*. Edward Arnold, 1st Edition, 1960.
- 86 Westerhof N, Stergiopoulos N, Noble MIM. *Snapshots of Hemodynamics*. Springer, 2nd Edition, 2010.
- 87 Nichols WW, O'Rourke MF, Vlachopoulos C. *McDonald's Blood Flow in Arteries. Theoretical, Experimental and Clinical Principles*. Hodder Arnold, 6th Edition, 2011.
- 88 Mancia G, De Backer G, Dominiczak A, Cifkova R, Fagard R, Germano G,; Grassi G, Heagerty AM, Kjeldsen SE, Laurent S, Narkiewicz K, Ruilope L, Rynkiewicz A, Schmieder RE, Boudier HAJ, Zanchetti A. 2007 Guidelines for the Management of Arterial Hypertension: The Task Force for the Management of Arterial Hypertension of the European Society of Hypertension (ESH) and of the European Society of Cardiology (ESC). *J of Hypertens* 2007; 25: 1105-1187.
- 89 Wesseling KH, Jansen JRC, Settels JJ, Schreuder JJ. Computation of aortic flow from pressure in humans using a nonlinear, three-element model. *J Appl Physiol* 1993; 74(5): 2566-2573.
- 90 Jellema WT, Wesseling KH, Groeneveld BJ, Stoutenbeek CP, Thijs LG, van Lieshout JJ. Continuous Cardiac Output in Septic Shock by Simulating a Model of the Aortic Input Impedance. A Comparison with Bolus Injection Thermodilution. *Anesthesiology* 1999; 90: 1317-1328.
- 91 Tyberg JV, Bouwmeester JC, Shrive NG, Wang JJ. CrossTalk opposing view: Forward and backward pressure waves in the arterial system do not represent reality. *J Physiol* 2013; 591(5): 1171-1173.
- 92 Hughes AD, Parker KH. CrossTalk: Forward, backward pressure and wave intensity. *Published on line April 10, 2013* Comments on the CrossTalk proposal and opposing view: Forward and backward pressure waves in the arterial system do/do not represent reality. *J Physiol* 2013; 591(5): 1167-1177.
- 93 Vermeersch SJ, Rietzschel ER, De Buyzere ML, Van Bortel LM, Gillebert TC, Verdonck PR, Segers P. The reservoir pressure concept: the 3-element windkessel model revisited? Application to the Asklepios population study. *J Eng Math* 2009; 64: 417-428.
- 94 Tyberg JV, Shrive NG, Bouwmeester JC, Parker KH, Wang JJ. The reservoir-wave paradigm: potential implications for hypertension. *Curr Hypertens Rev* 2008; 4: 203-213.
- 95 Lydakis C, Momen A, Blaha C, Herr M, Leuenberger UA, Sinoway LI. Changes of elastic properties of central arteries during acute static exercise and lower body negative pressure. *Eur J Appl Physiol* 2008; 102: 633-641.
- 96 Davis SC, Westerhof BE, van den Bogaard B, Bogert LW, Truijzen J, Kim YS, Westerhof N, van Lieshout JJ. Active standing reduces wave reflection in the presence of increased peripheral resistance in young and old healthy individuals. *J Hypertens* 2011; 29: 682-689.
- 97 Laskey WK, Kussmaul WG. Arterial wave reflection in heart failure. *Circulation* 1987; 75: 711-722.
- 98 Chirinos JA, Kips JG, Jacobs DR, Brumback L, Duprez DA, Kronmal R, Bluemke DA, Townsend RR, Vermeersch S, Segers P. Arterial wave reflections and incident cardiovascular events and heart failure: MESA (Multiethnic Study of Atherosclerosis). *J Am Coll Cardiol* 2012; 60: 2170-2177.

Professor Kim Parker's website at Imperial College, London, UK is the appropriate source for further details about the reservoir-wave theory.



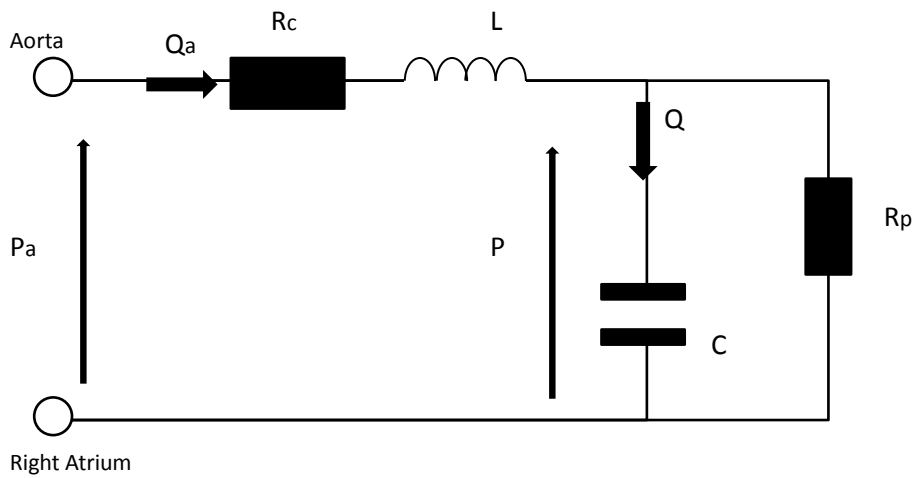
2-E WK

Figure 1 Diagram of a 2-E WK model: R and C are the resistance of the microcirculation and the compliance of the arteries.



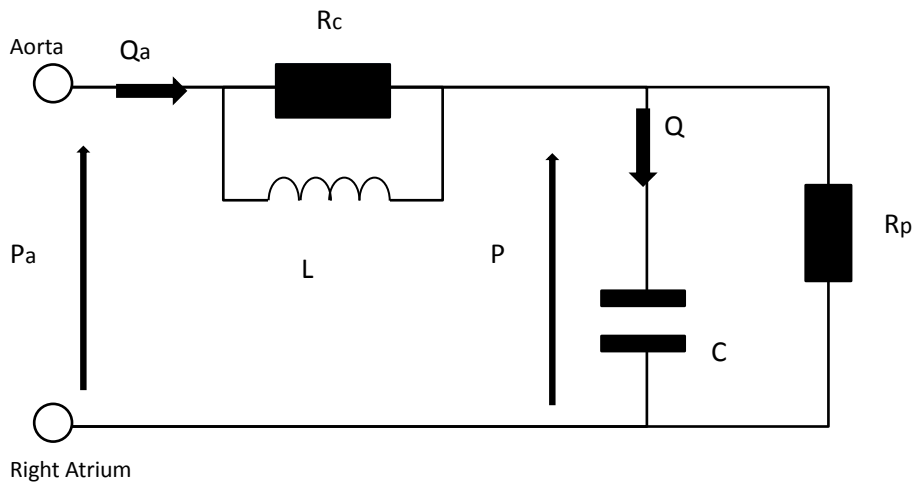
3-E WK

Figure 2 Diagram of a 3-E WK model: R_c is the characteristic impedance of the aorta in the absence of wave reflections; R_p is the peripheral resistance; C is the arterial compliance.



4-E WK

Figure 3 Diagram of a 4-E WK model: L and R_c are in series. L is the inertance of blood and consists of the sum of all local inertances of the arterial system. R_c is the characteristic impedance of the aorta in the absence of wave reflections; R_p is the peripheral resistance; C is the arterial compliance.



Modified 4-E WK

Figure 4 Diagram of the modified 4-E WK model: L and R_c are in parallel. L is the inertance of blood and consists of the sum of all local inertances of the arterial system. R_c is the characteristic impedance of the aorta in the absence of wave reflections; R_p is the peripheral resistance; C is the arterial compliance.

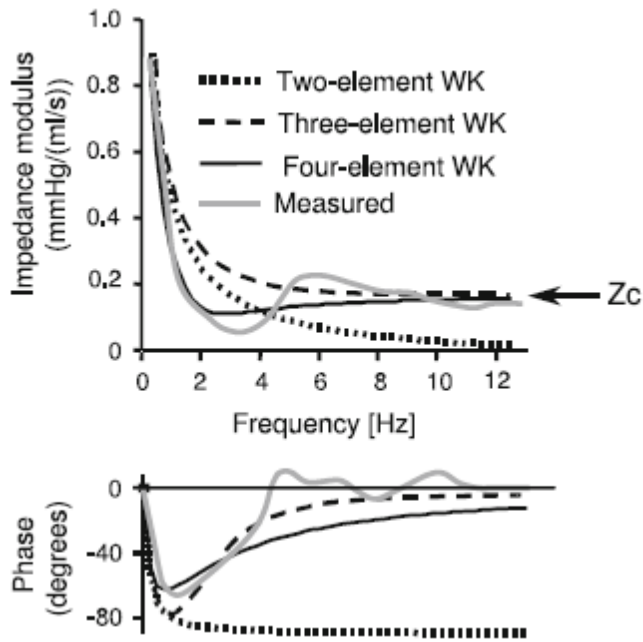


Figure 5 Comparison of measured aortic input impedance with values predicted by the 2-element, 3-element and 4-element windkessel model. Reprinted from: Westerhof N, Lankhaar J-W, Westerhof BE. *Med Biol Eng Comput* 2009; 47: 131-141.

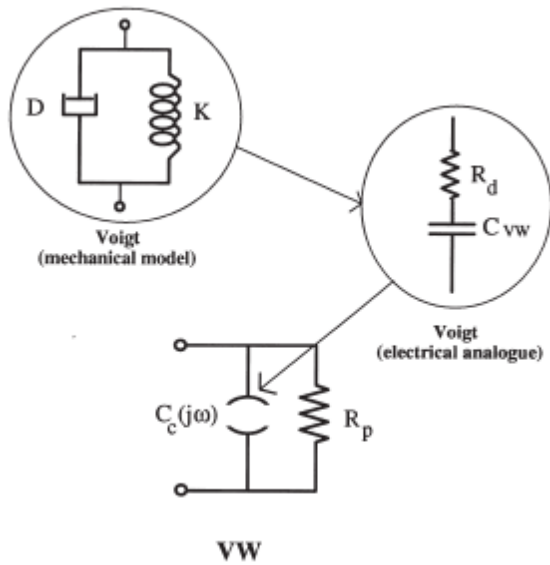
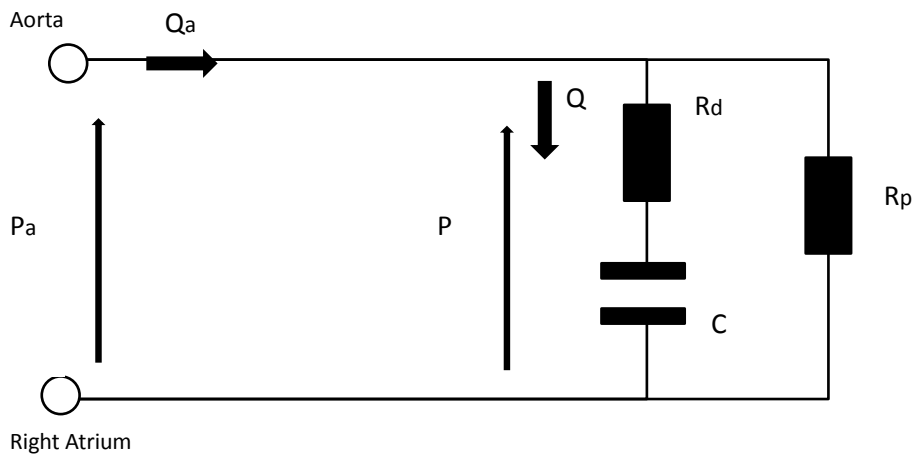
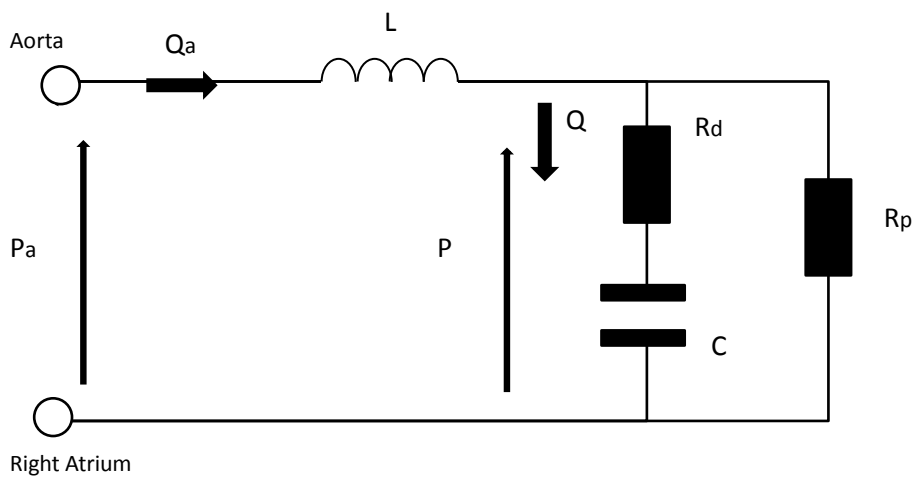


Figure 6 Electric analogue of the viscoelastic Windkessel model (VW) derived from a Voigt cell. Reprinted from: Burattini R, Natalucci S. *Medical Engineering & Physics* 1998; 20: 502-514 with permission from Elsevier.



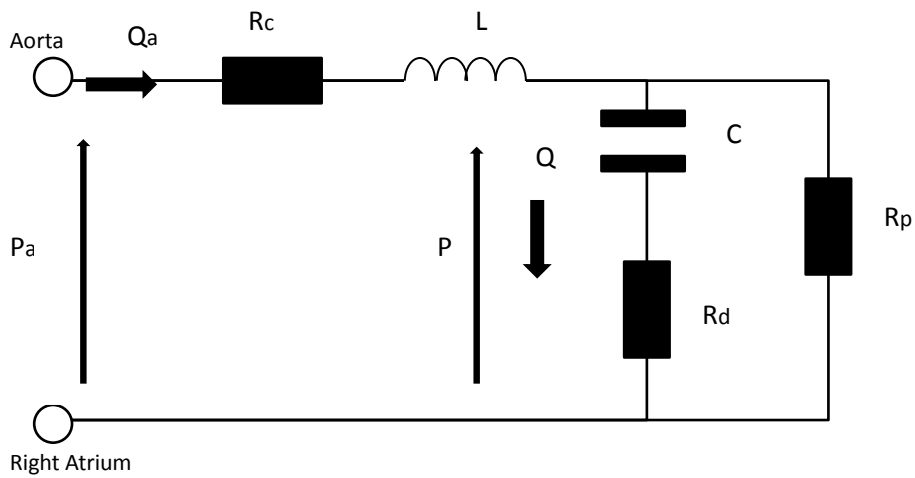
VW

Figure 7 Electric analogue of the viscoelastic Windkessel model (VW). R_d is a resistor accounting for viscous losses of wall motion. R_p is the peripheral resistance; C is the arterial compliance.



IVW

Figure 8 Electric analogue of the IVW model. R_d is a resistor accounting for viscous losses of wall motion. L is the inductance of blood and consists of the sum of all local inertances of the arterial system. R_p is the peripheral resistance; C is the arterial compliance.



Modified IVW

Figure 9 Modified IVW model. R_d is a resistor accounting for viscous losses of wall motion. L is the inductance of blood and consists of the sum of all local inductances of the arterial system. R_c is the characteristic impedance of the aorta in the absence of wave reflections; R_p is the peripheral resistance; C is the arterial compliance.

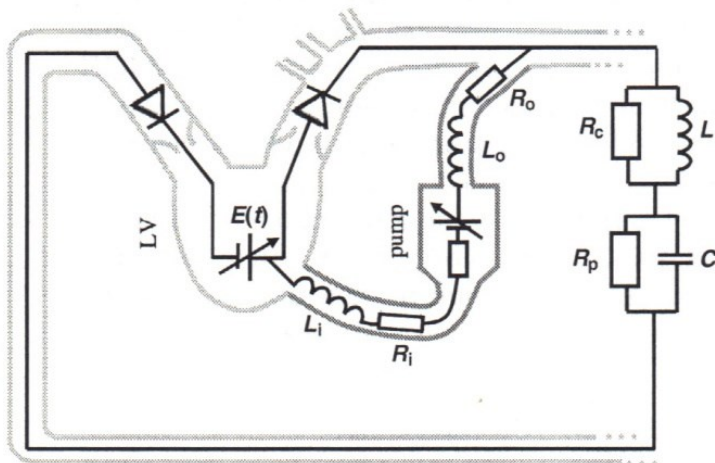


Figure 10 Electric analog of LVAD model coupled with the circulation: LV, rotary blood pump in parallel and 4-element windkessel. From: Artificial Organs 2002; 26(12): 1032-1039 with permission from John Wiley and Sons.